A Multipurpose and Reconfigurable mm-Wave Scanner System for Accurate Measurements of Passive/Active Antenna array, Array Calibration, Radome and Material Characterization

Jorge L. Salazar-Cerreno, Zeeshan Qamar, and Nafati Aboserwal
Advanced Radar Research Center (ARRC) & School of Electrical and Computer Eng. (ECE)
The University *of* Oklahoma, Norman, Oklahoma, USA.

***Abstract*—In this paper, the design, implementation and validation of a mm-Wave multipurpose system to perform antenna measurements, active antenna array calibration, material characterization, and radome testing is presented. The proposed system was developed based on a modular architecture that shares one set of instrumentation and two sets of antenna probes for five different operation modes without the need of changing the setup. This novel configuration enables a flexible, unique, and cost-effective solution for mm-Wave applications that operate from 75 GHz to 110 GHz. The proposed scanner includes a visual interface that guarantees autonomous operation permitting accurate measurements in all operational modes. The scanner was implemented and validated using different mm-Wave components, providing highly accurate measurements for each mode. Measured results for near-field, far-field, material and radome tests present excellent agreement with simulation results.**

***Index Terms*—Antenna measurements; active array calibration; automated mm-Wave system; near-field and far-field antenna measurements; material characterization; multipurpose; radome test and 5G.**

I. Introduction

Currently, the number of wireless applications are designed in mm-Wave frequency range [2]–[4]. These applications have components such as antennas, active arrays, filters, substrates, radomes, and other parts that require accurate automated characterization. To test and characterize these mm-Wave components, different scanners have been developed to operate in far-field or in near-field mode [5], [6]. The selection of which mode used depends on the antenna under test (AUT), space, and budget. For mm-Wave applications, far-field measurements are cost-effective and simple to implement. However, far-field mode requires space to measure the AUT. To overcome space constraints in far-field mode, NF-planar test ranges allow electrically large antennas to be measured within a smaller environment [5]. An interesting approach that offers flexibility to perform different antenna modes in the near-field region using a probe mounted on a robotic arm was presented in [7], [8]. This system is highly flexible and enables the measurement of integrated antennas at frequencies above 100 GHz to 280 GHz. A mm-Wave range system for embedded antennas in [9] uses a planar near-field setup to retrieve direct amplitude and phase values to measure the radiation pattern of only system embedded antennas.

Characterization of materials and radomes to be used in the mm-Wave region is critical for the development of front-end systems. Radome and materials, in this frequency range, are characterized and tested using the free-space method [10], [11]. This technique requires an automated measurement setup in which the frequency extenders and material under test require precise alignment. [10], [12].

Most of the existing mm-Wave scanners for antenna, radome or material tests are systems developed to use their own setups, space, and instrumentation. Taking into consideration that the mm-Wave equipment, cables, waveguides and antenna probes are extremely expensive, having a dedicated set for each operation mode is not cost-effective. Moving equipment from one setup to another for different modes of operation increases the risk of damage to the equipment and adds personnel and operational costs. In this paper a novel design for a mm-Wave test that enables multiple modes of operation is presented. The multipurpose proposed mm-Wave scanner consists of a modular design that allows the use of the same hardware, instruments, and software to perform five different tests in a frequency range from 75 GHz to 110 GHz. The system can perform antenna measurements in the modes of near-field planar (NFTM), far-field (FFTM), active array calibration (ACTM), material characterization (MTM), and radome testing (RTM). For all modes of operation, the system shares the same hardware, software, probes, and most importantly, the instrumentation. This allows using only one set of instrumentation in a multitasking system that is ideal for reducing both costs and physical space requirements. To guarantee autonomous operation permitting the system to accurately perform in all modes, a control software was implemented in NI-Labview. The graphic interface and post-processing software facilitate a user friendly operation that guarantees repeatable and reliable measurements.

Authors are with the Phased Array Antenna Research and Development (PAARD) group, the Advanced Radar Research Center (ARRC) and the Department of Electrical and Computer Engineering, The University of Oklahoma, Norman, OK, 73019 USA. Website: http://www.ou-arrc-paard.com
Manuscript received November 30, 2021

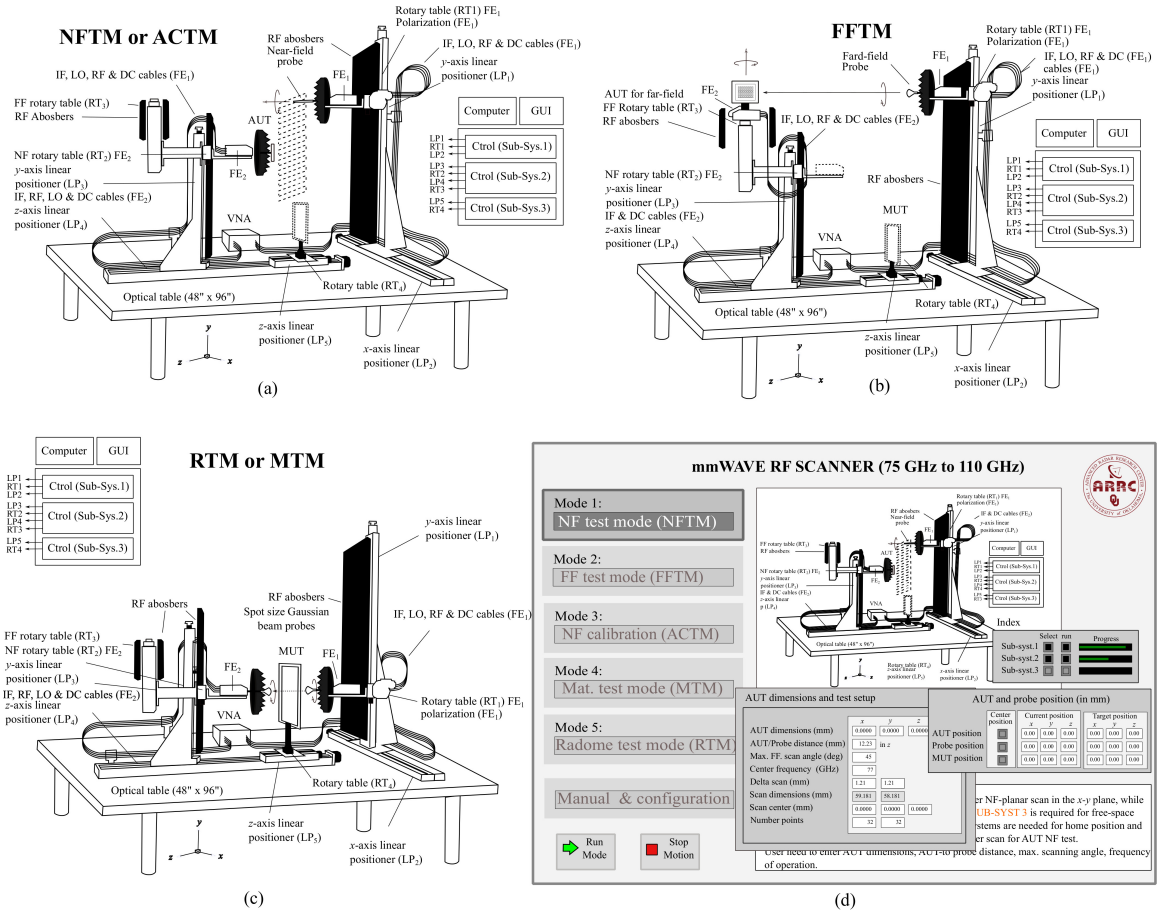

Fig. 1. Description of the multipurpose mm-Wave scanner modes. a) Near-field planar antenna test mode (NFTM) and active array calibration test mode (ACTM). b) Far-field antenna test mode (FFTM). c) Material and radome test modes (MTM and RTM), and d) Example of graphic user interface for NFTM.

TABLE I
GENERAL SPECIFICATIONS OF THE PROPOSED MULTIPURPOSE MM-WAVE SYSTEM.

Parameters	NFTM	ACTM	FFTM	MTM	RTM
Freq. operation	75-110 GHz	75-110 GHz	75-110 GHz	75-110 GHz	75-110 GHz
Max. scanning range	500×500 mm^2	500×500 mm^2	0° to 360°	-45° to +45°	-45° to +45°
AUT-probe separation	0-0.5 m	0-0.5 m	0-1.5 m	0-0.3 m	0-0.3 m
Max. DUT size	500 mm	500 mm	370×470 mm^2	304×457 mm^2	304×457 mm^2
Max. load capacity	90 kg	90 kg	20 kg	20 kg	20 kg
Position accuracy	0.076 mm	0.076 mm	100 arc-sec$^{(1)}$	100 arc-sec	100 arc-sec
Repeatability	0.0002 mm	0.002 mm	1 arc-sec	1 arc-sec	1 arc-sec
Graphic interface	yes	yes	yes	yes	yes
Safety mode	yes	yes	yes	yes	yes

$^{(1)}$ Units in arc-sec (1 arc-sec = 1/3600 of 1°)

II. MODES OF OPERATION

The five modes of operation listed below share the same hardware and instrumentation. Fig. 1 illustrates the general architecture of the proposed scanner for each individual mode, and Table I provides general specifications of the proposed system. In this system, every mode shares one vector network analyzer (VNA), model C4209 (100 kHz to 9 GHz), with CobaltFx frequency extenders (FE) that provide operation from 75 GHz to 110 GHz, two sets of probe antennas, one power supply, nine controllers, and one computer. The modes of operation proposed are:

1) Near-field planar test mode (NFTM)
2) Active array antenna calibration test mode (ACTM)
3) Far-field antenna test mode (FFTM)
4) Material test mode (MTM)
5) Radome test mode (RTM)

A. Scanner and control system

The multipurpose mm-Wave scanner has a total of 9-independent controllers, six of them is used for linear positioners and is of them are used for rotary tables. As illustrated in Fig. 1, the three subsystems are defined based on their functions and control configurations. All subsystems are implemented on an optical table of 1.2 m × 2.4 m that enables independent movement of each subsystem on its surface. This facilitates flexibility for each subsystem for new test configurations. Independent racks were designed to hold a set of cables for IF/RF, power, and control for each subsystem. Subsystem 1, an inverted tower and rail, is

known as an inverted T configuration. This configuration is excellent for accuracy, rigidity, and RF multi-path mitigation. Subsystem 1 controls the linear positioners 1 and 2 (LP_1 and LP_2) and rotary table 1 (RT_1). This subsystem enables fixed positions of antenna probe 1 and FE_1 in the x- and y-axis, and in far-field, radome or material test modes. Also, it defines an arbitrary position for near-field or calibration test modes. Rotary table 1 (RT_1) enables polarization rotation (0-360°) of antenna probe 1. Subsystem 2 has 4 controls, one for linear positioner 3 (LP_3) that moves the FE_2 (with AUT or probe) in the y-axis, the other for linear positioner 4 (LP_4) that moves the FE_2 (with AUT or probe) in the z-axis and rotary table 2 (RT_2). Rotary table 2 (RT_2) enables polarization rotation (0-360°) of FE_2 (with AUT and antenna probe 2). This polarization rotation is used in near-field planar mode, near-field array calibration, and material and radome test modes. Subsystem 3 is used exclusively for material and radome tests. Linear positioner 5 (LP_5) is used to center the radome or the material under test between probe 1 and probe 2. Rotary table 4 (RT_4) is used for material and radome tests as a function of the incident angle in azimuth plane. Two sets of antennas (2 lens corrected and 1 open-ended wave-guide probe) are used for near-field, far-field, and material characterizations, and radome and material tests. Software developed using NI-Labview was implemented to integrate the scanner, controllers, VNA/FEs, and MATLAB post-processing algorithms for each mode. A graphic user interface designed for ease of use for each mode of operation of the proposed system is also developed. This includes a control mode for manual operation and maintenance. Post-processing options including fast Fourier transform (FFT) processing, phase retrieval, probe correction, holographic projections for near-field antenna and calibration modes are available. Fig. 1d illustrates the visual interface for the NF AUT test mode and its main features. Table I describes specifications of the system for different modes. High-performance broadband absorbers (C-RAM SFC3) made from low-density polyurethane were used to cover metallic parts of the system.

III. Measurements System Validation

A. Near-field antenna test mode (NFTM)

For NF planar test mode, 3λ was used as a distance between the probe (in the FE_1) and the AUT antenna. This distance enables a $\pm 40°$ field of view with a scan window of 60 mm $\times$ 60 mm. In the near-field measurement, the W-band pyramidal horn antenna (SAR-2013-10-S2) that operates from 75 GHz to 110 GHz used as AUT. The antenna offers 20 dBi nominal gain and a typical half power beamwidth of 16 degrees in the E-plane and 18 degrees in the H-plane at the center frequency. The antenna supports linearly polarized waveforms. The input of this antenna is a WR-10 waveguide with UG-387/U-M. Fig. 2a,b presents 2D measured results of the magnitude and phase of co-polar patterns at 77 GHz in near-field region. Fig. 2c,d are the E- and H-cuts of the far-field antenna patterns overlapped with simulated results obtained using Ansys/HFSS. The simulated and measured radiation patterns of the horn antenna in E- and H-plane are in good correspondence in a field of view of $\pm 40°$ with an absolute error of 1.5 dB.

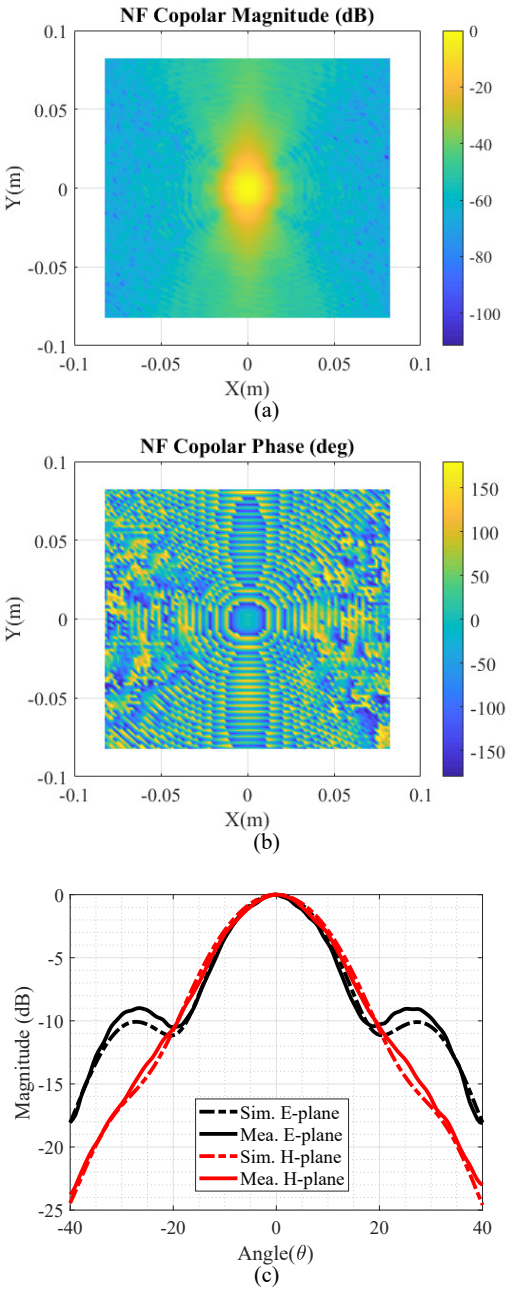

Fig. 2. Measured radiation patterns of a rectangular pyramidal horn antenna at 77 GHz tested in the near-field planar mode. a-b) 2D representation of the magnitude and phase of antenna patterns in the near-field region, respectively. c) HFSS simulated and measured antenna patterns for E- and H-plane.

B. Near-field array calibration test mode (ACTM)

In this mode of operation, an active array of 6×8 elements at 77 GHz with 8 analog phase-shifters and a single transmit and receive module for power and gain were characterized and calibrated using NF test modes. The active array, used as an AUT, is connected to the FE_2 using a 1 mm coaxial to WR-10 waveguide transition. The linear positioners LP_2 and LP_4 in subsystem 2 define the center of NF planar scan in the x-y plane. The separation between array and probe is 3λ. Since the antenna is polarized in y-axis, Ludwig 2-II is used to obtain the co-polar patterns [13], [14]. Linear positioners (LP_1, LP_2, LP_3, and LP_4) with a accuracy of 0.076 mm and repeatability of 0.0002 mm enable precise

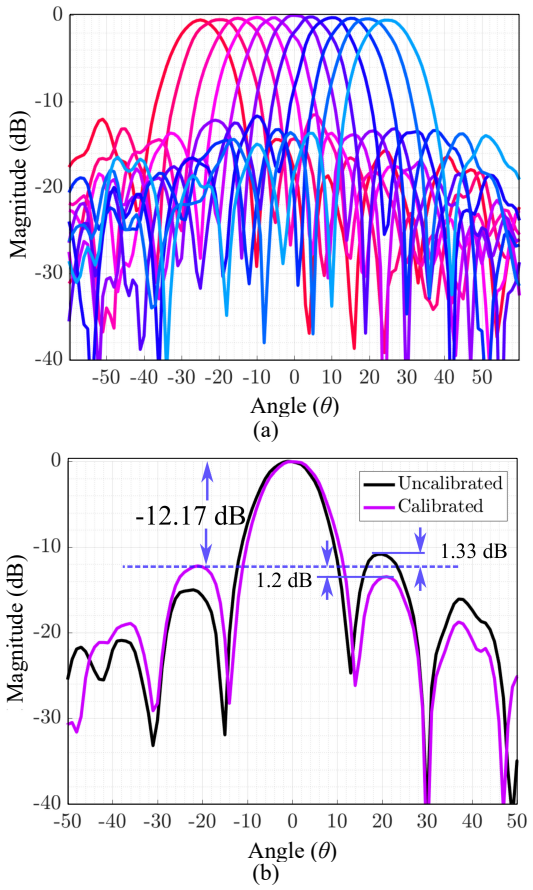

Fig. 3. Measured patterns of an active array of 6×8 elements at 77 GHz with 8 analog phase shifters. a) E-scanned beam patterns in H-plane for a steering angle range from -25° to 25° in steps of 5° tested in far-field mode. b) Comparison between the uncalibrated and calibrated patterns at broadside.

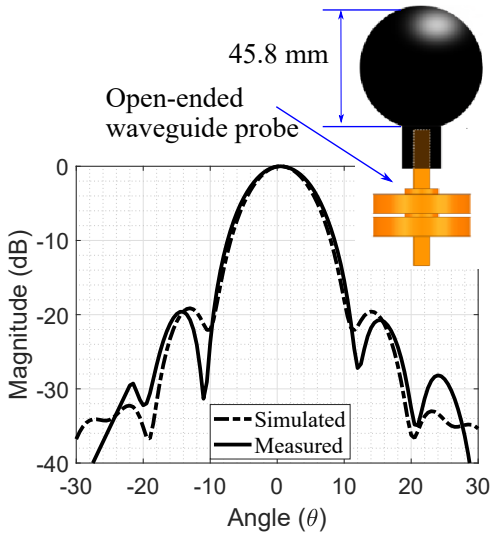

Fig. 4. Simulated and measured antenna patterns of the uniform dielectric lens antenna connected to a WR-10 waveguide used as a feed at 77 GHz.

sampling of the E-fields in the near-field region. Each column in the array acts as an active sub-array and is excited by an analog phase shifter, hence, for calibration purposes, the problem was reduced to test an 8-element linear array. Fig. 3b presents the broadside antenna patterns of the active array of 6×8 elements before and after calibration. This measurement was performed using FF mode. At broadside, a beam position error of ±1° with 1.3 dB deviation in the first sidelobe level was observed when the array was tested before calibration. Park-and-probe characterization in NF planar mode was used to characterize each sub-array. Knowing the power amplitude and phase deviation needed for ideal excitation in the array for each beam position, each analog phase shifter was adjusted for phased correction. Considering the active array did not have attenuators to correct amplitude errors, an optimization algorithm was used to identify the optimum combination of phase shifting that takes into account small-amplitude variations to obtain a better beam pattern for uniform distribution. Fig. 3a shows the measured results of electronically scanned (e-scanned) patterns after the calibration process. The e-scanned patterns, measured in FF mode, were obtained for a steering range from -25° to +25° and produced errors less than 0.01° for each beam position in the H-plane.

C. Far-field antenna test mode (FFTM)

A spherical uniform dielectric lens antenna was used to validate the far-field antenna test mode. The antenna was designed using Ansys/HFSS to operate at the center frequency of 77 GHz. Form-3 3D printer that uses the stereolithography (SLA) method was used to fabricate a lens antenna with a diameter of 45.8 mm. A cylindrical shape was added to support the antenna with the open-ended waveguide antenna used to excite the lens antenna. In this mode, the AUT fixture is mounted on top of FE_2, as shown in Fig. 1b. This fixture is composed of a Rohacell 51HF and a thin aluminum frame. Fig. 4 presents a comparison of the H-plane antenna patterns of the lens antenna tested in FF mode with simulated results obtained using HFSS. The absolute error of 0.9 dB was obtained between measured and simulated results of the lens antenna in the main beam region. However, small discrepancies were found in the region after ±10°. These discrepancies are attributed to not having a enclosed room with absorbers around the proposed scanner.

D. Radome test mode (RTM) and material test mode (MTM)

For RTM and MTM mode, both lens corrected antennas are mounted on FE's. as shwon in Fig 1c. The monolithic radome and materials (rogers 5880 and 4350B) are placed exactly at the center of the antennas. TRL calibration has been performed for accurate measurements. Fig. 5a illustrates the S-parameters of a monolithic (single layer) radome designed to operate at 82 GHz. S_{11} and S_{21} versus the frequency was overlapped with simulated results performed in HFSS. The S_{11} less than -20 dB were obtained for a frequency band from 78 GHz to 87 GHz. A maximum absolute error of 0.0031 dB was obtained in the radome measurements.

Fig. 5b,c shows the simulated and measured results of permittivity and tangent-loss, respectively, of RT-5880 and RO-4350B. The default materials from the HFSS library are used in the simulation to obtain their constitutive parameters. The measured permittivity is recorded as 2.16 and the tangent loss at 0.002-0.006 for the frequency band from 87.5 GHz to 92.5 GHz. For the Rogers 4350B, the permittivity equals to 3.50 and tangent loss ranges from 0.0033 to 0.006 are recorded. The maximum absolute error compared to expected

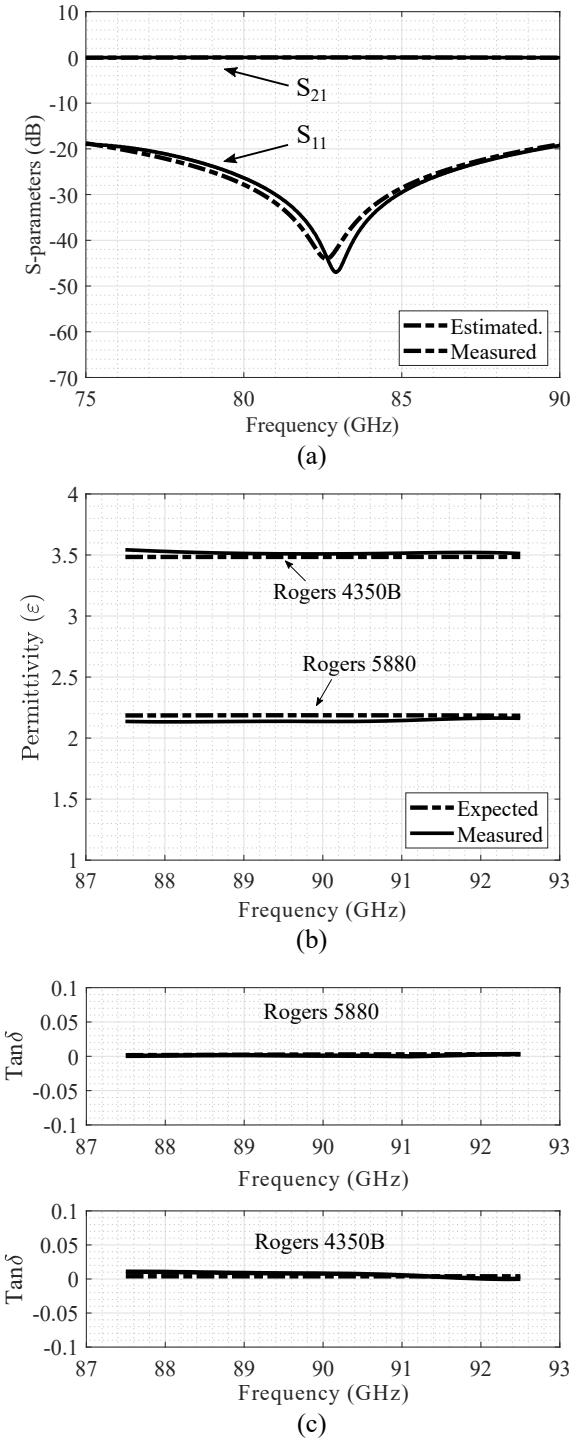

Fig. 5. (a) Simulated and measured s-parameters of a monolithic radome. (b-c) Simulated and measured permittivity and tangent-loss of Rogers 5880 and 4350B.

permittivities of both materials, Rogers 5880 and Rogers 4350B, are 0.03 and 0.02, respectively. In the case of tangent-loss, the maximum absolute error of Rogers 5880 is 0.0016 and Rogers 4350B is 0.003.

IV. Conclusion

In this work, a novel multipurpose scanner system is presented. The proposed system consists of a 9-axis fully automated scanner that enables antenna measurements in the near-field and far-field, active array calibration, material characterization, and radome testing. Design tradeoffs, implementation, and validation of the proposed scanner demonstrate this system is a cost-effective solution for mm-Wave applications that operate from 75 GHz to 110 GHz. A customized graphic interface enables fully autonomous operation and facilitates accurate, reliable, and repeatable measurements. Comparison between simulated and measured results of horn antenna and spherical dielectric lens antenna patterns were used to validate NF and FF test modes, respectively. The full calibration process of an electronically scanned active phased antenna array of 6×8 elements developed for 77 GHz automotive radar, demonstrates that the proposed system can be expanded for complex procedures. Accurate measurements of S-parameters of materials and a radome enable full characterization of permittivity, and tangent loss of various materials. Good agreement between measured and simulated results was found in all cases.

References

[1] authors, "title," blablabla.

[2] B. Bosco, R. Emrick, S. Franson, J. Holmes, and S. Rockwell, "Emerging Commercial Applications Using the 60 GHz Unlicensed Band: Opportunities and Challenges," IEEE Wirel. Microw. Technol. Conf. WAMICON 2006, pp. 6–9, 2006.

[3] J. Hasch, E. Topak, R. Schnabel, T. Zwick, R. Weigel, and C. Waldschmidt, "Millimeter-wave Technology for Automotive Radar Sensors in the 77 GHz Frequency Band," IEEE Trans. Microw. Theory Tech.,vol. 60, no. 3 PART 2, pp. 845–860, 2012.

[4] Z. Chen, Y. P. Zhang, A. Bisognin, D. Titz, F. Ferrero, and C. Luxey, "A 94-GHz Dual-Polarized Microstrip Mesh Array Antenna in LTCC Technology," IEEE Antennas Wirel. Propag. Lett., vol. 15, pp. 634–637, 2016.

[5] C. Parini, S. Gregson, J. McCormick, and D. J. Van Rensburg, "Theory and Practice of Modern Antenna Range Measurements" .IET, 2014,vol. 2.

[6] D. Slater, "Near-field Antenna Measurements". Artech House Antenna Library, 1991.

[7] L. Boehm, F. Boegelsack, M. Hitzler, and C. Waldschmidt, "The Challenges of Measuring Integrated Antennas at Millimeter-Wave Frequencies [Measurements Corner]," IEEE Antennas Propag. Mag.,vol. 59, no. 4, pp. 84–92, 2017.

[8] J. A. Gordon, D. R. Novotny, M. H. Francis, R. C. Wittmann, M. L.Butler, A. E. Curtin, and J. R. Guerrieri, "Millimeter-Wave Near-Field Measurements Using Coordinated Robotics," IEEE Trans. Antennas Propag., vol. 63, no. 12, pp. 5351–5362, 2015.

[9] Alonso-Delpino, Maria and Rosa, Marco Di and Simeoni, Massimiliano and Spella, Maristella and De Martino, Carmine and Spirito, Marco, "A Planar Near-field Setup for Millimeter-wave System-Embedded Antenna Testing," IEEE Antennas Wirel. Propag. Lett.,vol. 16, pp. 83–86, 2017.

[10] John W. Schultz, "Focused Beam Methods", Atlanta, 2012.

[11] Z. Qamar, N. Aboserwal, and J. L. Salazar-Cerreno, "An Accurate Method for Designing, Characterizing, and Testing a Multi-Layer Radome for mm-Wave Applications," IEEE Access, vol. 8, pp. 23 041–23 053, 2020.

[12] Hilario, Martin S. and Hoff, Brad W. and Jawdat, Benmaan and Lanagan, Michael T. and Cohick, Zane W. and Dynys, Frederick W.and Mackey, Jonathan A. and Gaone, Joseph M., "W-Band Complex Permittivity Measurements at High Temperature Using Free-SpaceMethods," IEEE Trans. Components, Packag. Manuf. Technol., vol. 9,no. 6, pp. 1011–1019, 2019.

[13] A. C. Ludwig, "The Definition of Cross Polarization," IEEE Transactions on Antennas and Propagation, pp. 116–119, 1973.

[14] N. A. Aboserwal, J. L. Salazar, J. A. Ortiz, J. D. Díaz, C. Fulton, and R. D. Palmer, "Source Current Polarization Impact on the Cross-Polarization Definition of Practical Antenna Elements: Theory and Applications," IEEE Trans. Antennas Propag., vol. 66, no. 9, pp. 4391–4406, 2018